PEGylation enables subcutaneously administered nanoparticles to induce antigen-specific immune tolerance

Peter Y. Li [a], Frank Bearoff [b], Pu Zhu [a], Zhiyuan Fan [a], Yucheng Zhu [a], Mingyue Fan [c], Laura Cort [b], Taku Kambayashi [d], Elizabeth P. Blankenhorn [b, *], Hao Cheng [a, c, *]

[a]Department of Materials Science and Engineering, Drexel University, Philadelphia, PA 19104, USA.

[b]Department of Microbiology and Immunology, Drexel University College of Medicine, Philadelphia, PA 19129, USA.

[c]School of Biomedical Engineering, Science and Health Systems, Drexel University, Philadelphia, PA 19104, USA.

[d]Department of Pathology and Laboratory Medicine, University of Pennsylvania Perelman School of Medicine, Philadelphia, PA 19104, USA.

*Corresponding Author.

Email: hcheng@drexel.edu (H. Cheng); eb29@drexel.edu (E. P. Blankenhorn)

ABSTRACT

The development of nanomaterials to induce antigen-specific immune tolerance has shown promise for treating autoimmune diseases. While PEGylation has been widely used to reduce host immune responses to nanomaterials, its tolerogenic potential has not been reported. Here, we report for the first time that a subcutaneous injection of PEGylated poly(lactide-co-glycolide) (PLGA) nanoparticles containing auto-antigen peptide MOG_{35-55} without any tolerogenic drugs is sufficient to dramatically ameliorate symptoms after disease onset in an antigen-specific manner in a mouse model of multiple sclerosis. Neither free MOG_{35-55} nor particles without PEG exhibit this efficacy. Interestingly, mechanistic studies indicate that PEGylation of nanoparticles does not reduce dendritic cell activation through direct nanoparticle-cell interactions. Instead, PEGylated nanoparticles induce lower complement activation, neutrophil recruitment, and co-stimulatory molecule expression on dendritic cells around the injection sites than non-PEGylated PLGA nanoparticles, creating a more tolerogenic microenvironment *in vivo*. We further demonstrate that the locally recruited dendritic cells traffic to lymphoid organs to induce T cell tolerance. These results highlight the critical role of surface properties of nanomaterials in inducing immune tolerance via subcutaneous administration.

Keywords: Immunotherapy, local immune modulation, immune cell recruitment, anergy, experimental autoimmune encephalomyelitis, biomaterials.

1. Introduction

Autoimmune disorders occur when the immune system loses self-tolerance and initiates an inflammatory immune response against healthy cells and tissues in the host [1]. Current therapeutic strategies either manage symptoms, as for type I diabetes, or globally suppress the immune system, as for multiple sclerosis (MS). Unfortunately, these treatments are usually lifelong and associated with a range of adverse effects [2, 3]. Therefore, recent research has directed its focus towards inducing antigen-specific tolerance, in which the immune system is trained to recognize a specific antigen as "safe", without attenuating immune protection against pathogens [4-7]. A variety of biomaterials-based strategies have been used in attempts to tolerize the immune system to an antigen of interest, sometimes in conjunction with tolerogenic drugs [8-12]. Existing studies that efficiently establish antigen-specific immune tolerance have largely employed systemic administration of engineered cells or nanomaterials carrying autoantigens [13-21]. Intravenously injected poly(lactide-co-glycolide) nanoparticles (PLGA-NPs) with conjugated or encapsulated antigen peptides with or without tolerogenic drugs have been shown to be efficacious in several autoimmune disease models. PLGA-NPs encapsulating gliadin protein (CNP-101/TAK-101) have shown promising results in a phase 2 clinical trial for treating celiac disease (NCT03738475). Although promising, translation of this or similar strategies to humans has yet to demonstrate efficacy in pivotal trials, and a fundamental understanding of how such biomaterials interact with the immune system is still lacking, necessitating the need for further study.

Although therapeutics can generally access immune cells more efficiently via systemic administration compared to subcutaneous (s.c.) injection, s.c. administration has advantages in convenience and ability to spatiotemporally modulate immune cells in a well-controlled microenvironment [12, 22-25]. One promising example is glatiramer acetate, one of the only FDA-

approved non-broadly immune-suppressing treatments for MS. The treatment is a s.c. injection of random peptide polymers of amino acids found in myelin, and it has shown moderate efficacy in humans [26, 27]. However, in efforts to increase antigen-specificity, current studies using s.c. administration of MS-relevant peptides alone or carried by NPs without additional drugs have not been able to ameliorate symptoms in experimental autoimmune encephalomyelitis (EAE), a well-characterized mouse model of MS [14, 15, 28]. Even with the incorporation of tolerogenic drugs or biomolecules into such NPs, most studies have only demonstrated efficacy by treating the disease before onset [29-34]. We hypothesized that this was in part a consequence of the inflammatory and/or stimulatory properties of the antigen-delivery materials after s.c. administration, and that tolerogenic responses could be achieved by modifying the intrinsic properties of the NP materials [35].

Recent studies have demonstrated that PLGA-NPs can cause inflammatory immune responses, including local recruitment of neutrophils and increased pro-inflammatory cytokines [36, 37]. Complement activation is one of the main drivers of biomaterials-induced inflammatory responses and immune activation [38-41]. Because the addition of polyethylene glycol (PEG) to NPs has been shown to reduce both protein adsorption and complement activation [42-44], we envisioned PEGylated NPs could induce a more tolerogenic systemic immune response. We then sought to directly compare the immune responses of PLGA-NPs versus their PEGylated counterparts. Consequently, we fabricated NPs using poly(lactic-co-glycolic acid)-*b*-poly(ethylene glycol) to encapsulate an EAE antigen peptide MOG_{35-55} (MOG-PLGA-PEG-NPs). We found that s.c. injections of these NPs into EAE mice after the onset of disease could dramatically decrease the severity of disease symptoms compared to mice treated with NPs without PEG or MOG_{35-55} alone (Fig. 1).

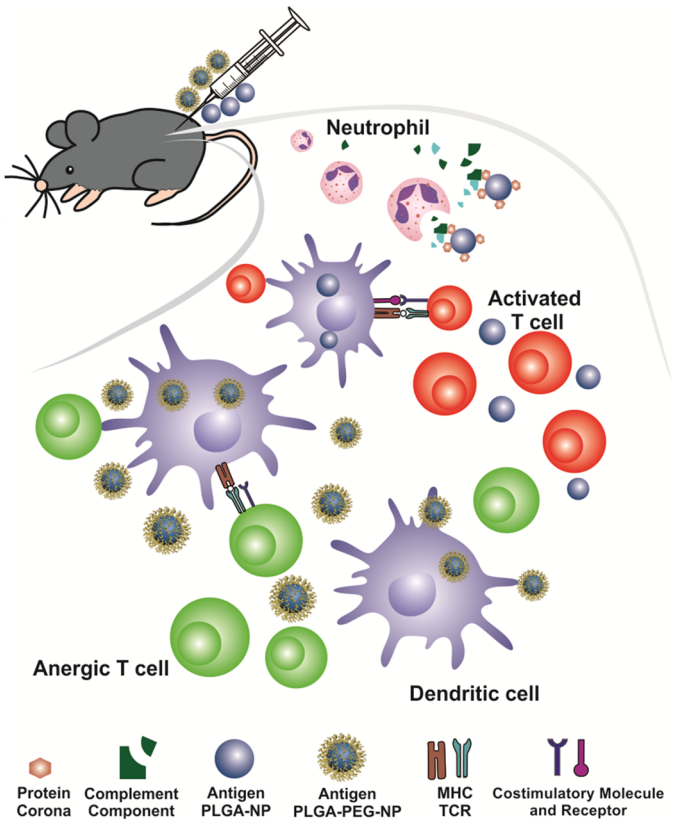

Fig. 1. Illustration of how PEGylated NPs can induce antigen-specific immune tolerance via s.c. administration in experimental autoimmune encephalomyelitis (EAE), a mouse model of multiple sclerosis. MOG-PLGA-NPs cause strong complement activation and stimulate dendritic cells, failing to ameliorate symptoms of EAE. Conversely, the PEG layer of MOG-PLGA-PEG-NPs with autoantigens significantly reduces NP-mediated complement activation and the expression of costimulatory molecules on dendritic cells, enabling tolerance induction.

To gain a better understanding of how the different NPs generated different immune responses, we studied their effect on immune cell activation, complement activation, biodistribution, and downstream T cell responses. Although the PEG layer did not make NPs more tolerogenic to antigen-presenting cells (APCs) *in vitro*, we found it reduced complement activation and co-stimulatory molecules on dendritic cells (DCs) *in vivo*, both locally and in the spleen. This corresponded to an increase in tolerogenic T cell responses systemically. Due to the ubiquity of PLGA-based nanomaterials for immunotherapy [45], the knowledge gained here may be helpful for the general design of biomaterials for immune tolerance.

2. Materials and methods

2.1 Nanoparticle Fabrication

Methoxy PLGA-PEG (PEG:PLGA 5,000:20,000 Da, Akina, West Lafayette, IN, catalog number AK037) NPs were fabricated via a double emulsion method as previously reported [46]. The polymer was dissolved in 20 mg/mL of dichloromethane (DCM) (Sigma-Aldrich, St. Louis, MO). MOG_{35-55} (RS Synthesis, Louisville, KY) was dissolved in 20 mg/mL de-ionized (DI) water. For the first emulsion, 45 µL of the MOG solution was added to 450 µL of the polymer solution and then sonicated using a probe sonicator (Fisher Sonic Dismembranator) for 12 s at 20% amplitude (pulse 1 s on/1 s off). Then, 1.35 mL of 1% w/v polyvinyl alcohol (PVA) (Sigma-Aldrich, St. Louis, MO) was added to the emulsion and sonicated again for 24 s using the same settings. The entire volume was then added to 6 mL of 0.1% PVA and stirred on a magnetic stir plate for 16 h at 750 rpm to evaporate the organic solvent. To remove the PVA, the NPs were washed by centrifuging 3 times at 18,000 × g for 7 mins and resuspending in DI water each time. For storage, MOG-PLGA-PEG-NPs were suspended in water, frozen at -80 °C, and thawed on the day of use.

To fabricate MOG-PLGA-NPs, a modified procedure was used due to the difficulty of resuspending non-PEGylated MOG-encapsulated NPs and to keep size and peptide loading consistent. For the first emulsion, 25 µL of MOG_{35-55} at 4 mg/mL in 0.5 M Tris-HCl (pH=8) was emulsified with 500 µL of 50:50 PLGA with inherent viscosity 0.66 (15,000-25,000 Da, Durect Inc., Cupertino, CA) dissolved in DCM at 10 mg/mL by probe sonicating for 20 s at 20% amplitude. To this, 5 mL of 10 mM Tris-HCl was added and the solution was sonicated for 40 s at the same settings. The entire emulsion was then transferred to a 20 mL vial and stirred for 16 h at 750 rpm to evaporate the organic solvent. The NPs were then washed by centrifuging twice at 15,000 ×g

for 7 min and resuspending in DI water after each centrifugation. MOG-PLGA-NPs were freshly prepared and stored in water at 4 °C for less than 24 h before injection due to aggregation during the thawing process if frozen.

To make fluorescently labeled particles, 0.05 wt% DiD (Thermo Fisher, Waltham, MA) dissolved in DCM was added to the polymer solution prior to the first emulsion. For the PLGA-PEG-NPs encapsulating $OVA_{323-339}$ (RS Synthesis, Louisville, KY), the peptide was dissolved at 10 mg/mL in water with 0.5% NH_4OH. For the first emulsion, 90 µL of peptide solution was added to 450 µL of PLGA-PEG in DCM and sonicated for 12 s. Subsequent steps were the same as for the fabrication of MOG-PLGA-PEG-NPs.

2.2 Nanoparticle characterization

NPs were imaged via transmission electron microscopy (TEM) using a JEOL JEM2100 TEM. Briefly, a carbon film-coated copper grid was cleaned by plasma, and 10 µL of NP solution was dropped on the grid. After incubating for 20 min, the grid was rinsed with 10 µL of DI water 3 times. Then 5 µL of 2% uranyl acetate water solution was dropped onto the grid and was immediately removed by a filter paper. The grid was then dried and imaged at 200 kV.

NP size and zeta potential were measured via dynamic light scattering (DLS, Zetasizer Nano ZS90). Protein encapsulation of the NP was determined via bicinchoninic acid (BCA) protein assay. Briefly, supernatants of the NP solution were collected and diluted 10× in water. The amount of protein was then measured using the Micro BCA Protein Assay Kit (Thermo Fisher, Waltham, MA) according to manufacturer instructions. This represented the amount of unencapsulated peptide, which was subtracted from the total initial amount to determine encapsulation.

2.3 Peptide release

Peptide release was determined by encapsulating fluorescein isothiocyanate (FITC)-conjugated MOG_{35-55} in PLGA or PLGA-PEG NPs. After fabricating the NPs and washing, the NPs were suspended at 2.5 mg/mL in release media, which consisted of PBS with 10% FBS and 1% penicillin/streptomycin (PS). The amount of encapsulation was determined by measuring the unencapsulated FITC signal after removing all the NPs in solution by centrifuging at 20,000 × g for 15 min and comparing to a known working line of fluorescence intensity and FITC-MOG peptide concentration. 400 μL of the NP suspension was placed in a 20K MWCO dialysis cup (Thermo Scientific, Waltham, MA), which was then immersed in 1 mL of the release media in a 1.5 mL tube and shaken at 100 rpm at 37 °C. At designated time points, the fluorescence of the release media was tested and replaced with fresh media. The release was calculated as a percentage of the initial encapsulated value.

2.4 Bone marrow-derived dendritic cell (BMDC) culture and NP treatment

BMDCs were cultured based on an established protocol [47]. Briefly, tibias and femurs from female C57BL/6J mice were isolated and placed in 70% ethanol for 2-3 min to sterilize them. The ends of the bones were then cut and the marrow was flushed with RPMI 1640 medium using a 29G syringe into a clean petri dish. The cells were disassociated by resuspending with a pipette tip. The cells were then centrifuged, and RBCs were removed using RBC lysis buffer (Biolegend, San Diego, CA). The resulting cells were cultured in 60 mm Petri dishes in RPMI 1640 with 10% FBS (ATCC, Manassas, VA), 1% penicillin/streptomycin (ATCC, Manassas, VA), 50 μM 2-mercaptoethanol (Thermo Fisher, Waltham, MA), and 20 ng/mL of GM-CSF (Peprotech, Rocky Hill, NJ) at a concentration of 2×10^6 cells per 5 mL medium. On day 3 of culture, 2 mL of medium

per dish was removed and replaced with 3 mL of fresh medium. On day 6, the loosely attached cells were replated with 5×10^5 cells in 1 mL of medium in a 24-well low-attachment plate. For flow cytometry cell analysis, NPs were added to the wells on day 7 at a concentration of 100 μg/mL, normalized based on the DiD signal of NPs. On day 8 or 9, the loosely attached cells were detached by gentle pipetting and collected for analysis. Alternatively, NPs without DiD or 1 μg/mL LPS was added for surface marker study. The flow cytometry gating strategy is shown in Fig. S1.

For confocal imaging studies, a clean #1.5 round cover glass (Harvard Apparatus, Holliston, MA) was pre-incubated with 0.01% poly-L-lysine solution (Sigma-Aldrich, St. Louis, MO) for 15 min at 37 °C, then rinsed twice with sterile water. The cover glasses were placed in 24-well plates. Cultured BMDCs were detached from plates on day 7 of culture and added to the wells with the cover glass along with 100 μg/mL of DiD-labeled NP. After 24 h, the culture supernatant was aspirated, and the cells were fixed with 2% paraformaldehyde (PFA) (Sigma-Aldrich, St. Louis, MO), rinsed with PBS, then stained with PE-conjugated anti-CD11c antibody (All surface marker antibodies were from Biolegend, San Diego, CA unless otherwise specified). After incubating for 1 h at RT, the cells were washed, counterstained with Hoechst stain (Sigma-Aldrich, St. Louis, MO) for 15 min, washed, then mounted on a glass microscope slide using anti-fading medium (EMD Millipore, Burlington, MA). Samples were imaged on an Olympus IX81 confocal microscope at 60× magnification.

2.5 EAE studies

To induce EAE, 10-week-old female C57BL/6J mice (The Jackson Laboratory, Bar Harbor, ME) were injected with an emulsion of MOG_{35-55} and complete Freund's adjuvant (CFA) (Sigma-Aldrich, St. Louis, MO), as well as 2 injections of pertussis toxin (PTX) (List Labs, Campbell,

CA), spaced 2 days apart. The emulsion was formed by probe sonicating a 1:1 ratio of MOG_{35-55} in PBS (2 mg/mL) and CFA (4 mg/mL) until it achieves the consistency of a thick paste. Each mouse was given two s.c.injections of 100 µL in the hind flanks for a total of 200 µg of MOG_{35-55} and 400 µg of CFA. At the time of the emulsion injection, 100 µL of PTX in PBS (175-200 ng) was injected i.p., which was repeated 2 days later. Beginning at day 9 after immunization, the mice were scored daily for clinical signs of disease. Scoring was performed on a 5-point scale: 0, no disease; 1, floppy tail; 2, hind limb ataxia; 3, hind limb paralysis; 4, front limb paralysis; 5, dead. For the NP efficacy studies, mice were injected s.c. in the back or via tail vein with 3 mg of NPs, corresponding to approximately 50 µg of MOG_{35-55} peptide, in 75 µL of PBS at the indicated time points. All animal procedures were conducted in accordance with the protocols approved by the Drexel Institutional Animal Care and Use Committee in compliance with NIH guidelines.

2.6 Injection-site cell analysis

C57BL/6J mice were injected with 3 mg of DiD-MOG-PLGA-PEG-NP or DiD-MOG-PLGA-NP in 100 µL PBS. After 48 h, the mice were sacrificed and the s.c.tissue in a 3 cm^2 area centered around the NP injection site was collected using tweezers. The tissue was digested using 250 U/mL of collagenase IV in RPMI 1640 for 30 min at 37 °C on a shaker at 100 rpm. The tissue was then mechanically separated and passed through a 70 µm cell strainer to collect the cells. Cells were counted and stained for flow cytometry. Cells were analyzed according to the gating strategy shown in Fig. S2.

2.7 *In vitro* measurement of complement activation

The sizes of MOG-PLGA-PEG-NP and MOG-PLGA-NP were determined via DLS and were used to calculate the weight of particles needed to achieve a desired total surface area based on a NP density of 1.2 g/cm^3 [43]. To test for complement activation, 0.0025 m^2 of NPs in 10 µL of water were added to 40 µL of normal human serum (Complement Technology, Inc., Tyler, TX) in a 96-well sterile cell-culture plate and incubated at 37 °C for 1 h. As a positive control, mouse IgG (Sigma-Aldrich, St. Louis, MO) was heat-aggregated at 70 °C for 30 min and added to the serum at a final concentration of 1 mg/mL. Zymosan (Complement Technology, Inc., Tyler, TX) was added to serum at a final concentration of 0.5 mg/mL. Complement activation was quenched by adding 12.5 µL of 0.05 M EDTA solution in PBS and the samples were transferred to clean 1.5 mL tubes. NPs were removed by centrifuging at 18,000 × g for 7 min and the supernatants were collected and tested for complement activation. ELISAs were performed using the MicroVue C4d and C5a EIA kits (Quidel, San Diego, CA) according to manufacturer instructions.

2.8 Western blotting analysis of complement activation *in vivo*

Western blot (WB) was applied to determine the difference of complement activation induced by PEGylated and non-PEGylated NPs *in vivo*. Briefly, DiD-MOG-PLGA-NPs and DiD-MOG-PLGA-PEG-NPs each at 3 mg in 100 µL H_2O were s.c. injected into different sides on the back of a C57BL/6 mouse. The NPs and NP-infiltrated subcutaneous tissues were collected 1h after injection and kept in 100 µL DPBS (Corning, Manassas, VA). A control group of subcutaneous tissue without any NPs was also collected as a control. NPs with infiltrated tissues and the spare tissue were centrifuged at 20,000 rcf for 20 min. The supernatant and pellet were added into Bio-Rad sample buffer containing β-mercaptoethanol, boiled at 95°C for 10 min and separated on 7.5-12.5% acrylamide gel. The proteins were then transferred to PVDF membrane overnight. After

blocking in 5% wt nonfat dry milk in PBS-T (1x PBS with 0.05% Tween-20) for 1h, the PVDF membrane was washed in PBS-T 3 times and incubated with recombinant anti-C3 antibody (Abcam, Cambridge, MA) at 1:2000 dilution for another 1h. The membrane was then incubated with goat anti-rabbit HRP (Invitrogen, Waltham, MA) at 1:2000 dilution for 40 min and probed using ProteinSimple (FluorChem E System).

2.9 DiD release from NPs

MOG-PLGA-PEG-NP and MOG-PLGA-NP containing 0.05 wt% DiD were fabricated as described above. After washing, NPs were suspended in 1 mL of PBS with 10% FBS and 1% penicillin/streptomycin and incubated at 37 °C on a shaker at 100 rpm. At determined time points, NPs were centrifuged in a 100K MWCO centrifuge tube (Amicon) and the filtered solution was tested for DiD signal. The NPs collected by the filter were resuspended in fresh release media and the procedure was repeated for the next time point.

2.10 Biodistribution studies

C57BL/6J mice were induced with EAE. At the onset of disease (score > 1), 3 mg of DiD-labeled MOG-PLGA-PEG-NPs or MOG-PLGA-NPs were s.c. injected into the upper backs of the mice. After 6-8 days, the mice were sacrificed, blood was removed by systemic perfusion of PBS, and the CNS (brain and spinal cord), spleen, and axillary and inguinal lymph nodes were collected. To create a single cell suspension of CNS leukocytes, the CNS was first minced and enzymatically digested using 300 µg/mL of Type IV Collagenase (Worthington) for 30 min at 37 °C. The softened CNS tissue was then mashed through a 70 µm cell strainer and washed with PBS. After centrifuging, the pellet was resuspended in 4 mL of 35% Percoll (GE) and then layered over 4 mL

of 70% Percoll. This was centrifuged for 15 min at 600 ×g without brakes, and the resulting interlayer between the two gradients was collected, containing the leukocyte cell population. This was washed and resuspended in media for subsequent analysis. Single cell suspensions of spleen and lymph node cells were obtained by mashing through a 70 µm cell strainer, lysing the RBCs, washing, and resuspending in media.

For flow cytometry, 2.5×10^5 or 1×10^6 cells were pelleted in a 1.5 mL tube and resuspended in flow buffer (PBS + 4% FBS) and incubated with anti-CD16/32 antibody for 10 min to prevent non-specific binding. The cells were then stained using various combinations of PE-CD11c, PE/Cy7-CCR7, APC/Cy7-Ly6G, PerCP/Cy5.5-MHC-II, FITC-F4/80, APC/Cy7-CD86, PE/Cy7-F4/80, and FITC-CD19. The cells were analyzed via flow cytometry on a BD FACS Canto.

2.11 Splenocyte antigen recall

To test the antigen recall ability of mouse splenocytes, the cells were cultured in a 24-well plate at a concentration of 1×10^6 cells/mL in RPMI media with 10% FBS, 1% penicillin/streptomycin, and 50 µM 2-mercaptoethanol, and challenged with 25 µg/mL MOG_{35-55}. After 3 days, the cells were collected, centrifuged, and stored in Trizol Reagent (Thermo Fisher, Waltham, MA) for further real-time PCR analysis. To perform qRT-PCR, a phenol-chloroform extraction was used to isolate RNA in the aqueous phase, The RNA was then precipitated in isopropyl alcohol and washed with 75% ethanol. After removal of the ethanol, the RNA pellet was resuspended in water and the TURBO DNA-free kit (Thermo Fisher, Waltham, MA) was used according to manufacturer instructions to remove any contaminating DNA. The amount of RNA was measured using a NanoDrop 1000 Spectrophotometer. The High-Capacity cDNA Reverse Transcription Kit (Thermo Fisher, Waltham, MA) was then used to create the cDNA. Forward and

reverse primers were obtained from IDT Technologies and used along with PowerUp SYBR Green Master Mix to perform the qRT-PCR on a QuantStudio 6 Flex Real-Time PCR System. The following primer sequences were used: IL-17a (F: TCCAGAATGTGAAGGTCAACC; R: TATCAGGGTCTTCATTGCGG), IL-22 (F: TCGCCTTGATCTCTCCACTC; R: GCTCAGCTCCTGTCACATCA), and GAPDH (F: CCAGAACATCATCCCTGCAT; R: GTTCAGCTCTGGGATGACCTT).

2.12 Ag-specific T cell and Treg analysis

To measure the immune cell populations of NP-treated mice, CNS and spleen cells were collected and surface stained as described previously with various combinations of PE/Cy7-CD4, APC/Cy7-CD3, PerCP/Cy5.5-CD8, APC-CD25, APC-I- PE-CD11c, FITC-F4/80, PE/Cy7-PDL1, PE-Ly6G, PerCP/Cy5.5-MHC-II, and APC/Cy7-CD86 antibodies, and APC-I-A(b) human $CLIP_{87-101}$ tetramer and APC-I-A(b)MOG_{38-49} tetramer (NIH Tetramer Core Facility). The only exception was for samples that required tetramer staining, which was performed before other surface stains. Briefly, after the addition of blocking antibody, the samples were stained with tetramer at a concentration of 2 μg/mL/million cells for 2 h at 37 °C. Then, the remaining surface stains were performed using the standard staining protocol at 4 °C. Flow cytometry analysis was performed by comparing to an irrelevant human tetramer control (Fig. S3). Intracellular PE-conjugated FoxP3 staining (Thermo Fisher, Waltham, MA) was performed according to manufacturer instructions using the eBioscience Mouse Regulatory T Cell Staining Kit. Cells were analyzed according to the gating strategy shown in Fig. S4.

2.13 Statistical analysis

Data analysis was performed using GraphPad Prism software (GraphPad Software, San Diego, CA). Student's t-test (Two-Sample Assuming Equal Variances) was used to analyze statistical significance between two groups. EAE efficacy data was analyzed using two-way ANOVA with post-hoc Tukey's test and reported for the last data point. Sample sizes are indicated in each Fig. and were chosen based on preliminary data and comparable published studies. A value of $p < 0.05$ was considered statistically significant.

3. Results and discussion

3.1 Fabrication and characterization of NPs

MOG-PLGA-PEG-NPs and MOG-PLGA-NPs were fabricated via double emulsion (Fig. 2A). The method was adjusted to ensure both NPs had similar average sizes between 250-300 nm as measured by dynamic light scattering (Fig. 2A) and had similar MOG_{35-55} loading capacity, ~11-19 μg/mg of polymer in both NPs (Fig. 2B). MOG-PLGA-PEG-NPs showed a faster release profile of encapsulated MOG_{35-55} compared to MOG-PLGA-NPs (Fig. 2C). This is possibly because of the hydrophilic domains of PEG trapped inside PLGA core [43], generating shortcuts that enabled a faster diffusion of water-soluble MOG_{35-55} inside particles.

Because the PEG layer around NPs can interfere with the ability of cells to internalize NPs, BMDCs were used to verify that the PEGylated NPs can still be effectively internalized. BMDCs were incubated with DiD-labeled MOG-PLGA or MOG-PLGA-PEG NPs at 100 μg/mL *in vitro* for 24 h and then analyzed via confocal microscopy and flow cytometry. Although cells internalized more MOG-PLGA-NPs than MOG- PLGA-PEG-NPs (Fig. 2D, E, S5), the percentages of BMDCs ($CD11c^+$) that internalized NPs were higher than 95% for both conditions (Fig. 2E).

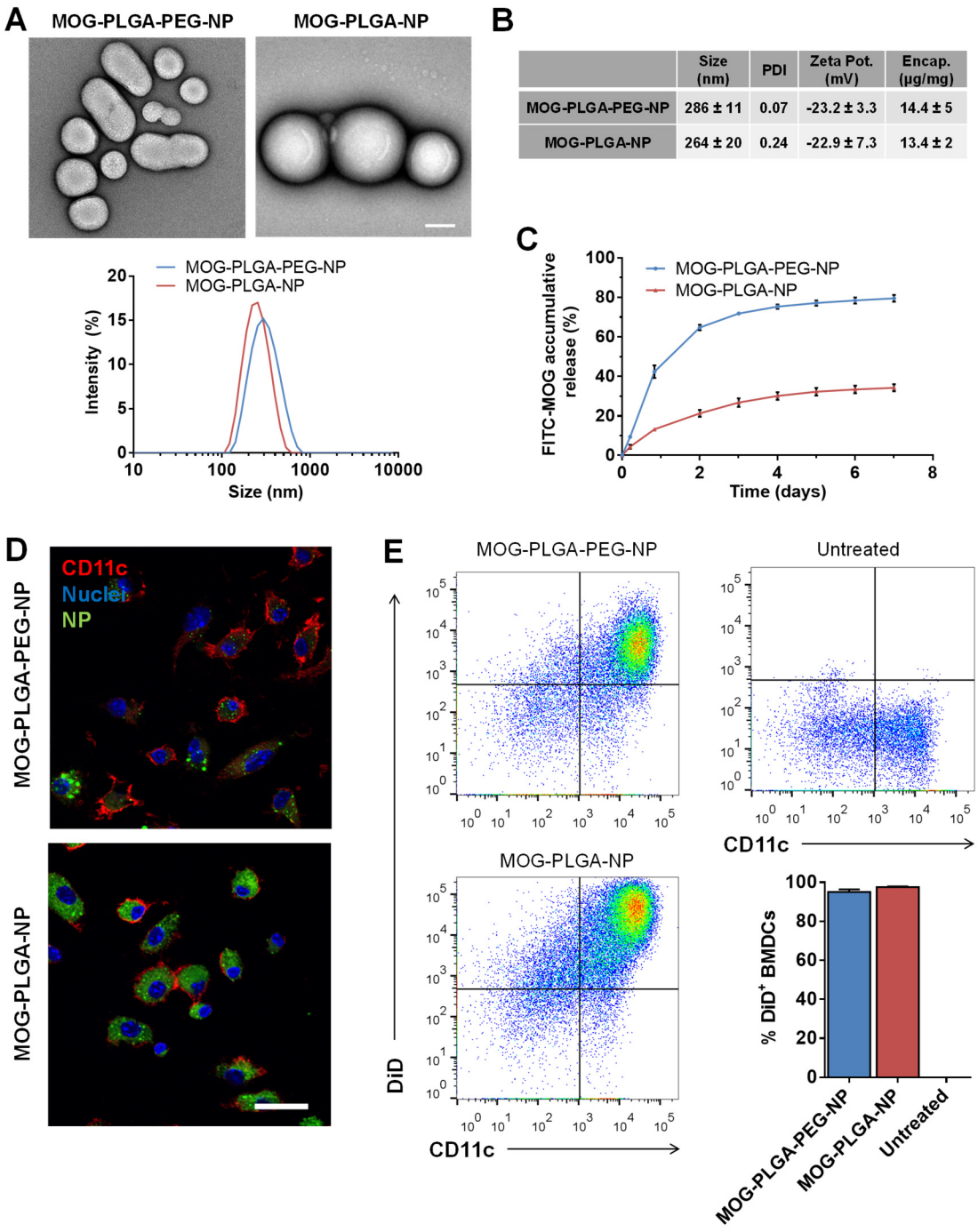

	Size (nm)	PDI	Zeta Pot. (mV)	Encap. (µg/mg)
MOG-PLGA-PEG-NP	286 ± 11	0.07	-23.2 ± 3.3	14.4 ± 5
MOG-PLGA-NP	264 ± 20	0.24	-22.9 ± 7.3	13.4 ± 2

Fig. 2. Nanoparticle characterization and uptake by BMDCs. (A) Representative TEM images and DLS size distribution of NPs, scale bar = 100 nm. (B) NP physical properties. (C) Release of encapsulated FITC-MOG from NPs. (D) Representative confocal microscopy images of BMDCs treated with NPs. BMDCs were cultured with 100 µg/mL of DiD labeled MOG-PLGA-PEG or MOG-PLGA-NPs (green) for 24 h, then stained for CD11c (red) and nuclei (blue). Scale bar = 20 µm. (E) Flow cytometry analysis of BMDCs treated with NPs. Dot plots are the representative raw data of CD11c expression and DiD signal of BMDCs. Data are represented as mean ± S.D. (n=3).

3.2 PEGylated NPs ameliorate EAE in an antigen-specific manner

To test whether PEGylation of NPs has an effect on their ability to induce tolerance when subcutaneously injected in an autoimmune disease mouse model, EAE resembling progressive MS was induced in C57BL/6J mice. The mice were then given a s.c. injection of 3 mg of various NPs or a similar amount of MOG_{35-55} in PBS at the onset of disease and again 5 days later. Clinical disease severity in the mice was scored on a scale of 0-5, with 0 = no disease, 1 = tail limp, 2 = hindlimb ataxia, 3 = hindlimb paralysis, 4 = forelimb paralysis, and 5 = death. Mice treated with MOG-PLGA-PEG-NPs began to exhibit disease remission within 5 days of the initial NP injection. The average score dropped to less than 0.5 before some mice showed a relapse starting around day 30, leveling out to an average score of 1 at day 41 (Fig. 3A). In contrast, the clinical scores of mice treated with MOG-PLGA-NPs or soluble MOG remained at an average of around 2.5. MOG-PLGA-PEG-NPs alleviated the disease symptoms in an antigen-specific manner as the mice showed a higher clinical score when treated with NPs (OVA-PLGA-PEG-NPs) encapsulating an EAE-irrelevant antigen, $OVA_{323-339}$.

We next tested whether pretreatment before disease onset would change the efficacy of the MOG-PLGA-PEG-NPs. When MOG-PLGA-PEG-NPs were s.c. injected at days 5 and 10 after disease induction, the mice exhibited symptoms (disease onset) later and more gradually, with no rapid peak as seen in the PBS control. Eventually, the mice reached an average score of around 1 (Fig. 3B), which was similar to the score of the mice treated after disease onset. This suggests that s.c. injected MOG-PLGA-PEG-NPs may prevent severe disease. However, other components such as tolerogenic drugs may still be needed to modulate immune cells for reversing the course of autoimmunity completely. For instance, rapamycin and TGF-ß have demonstrated the ability to enhance the tolerogenic effect of nanoparticles [16, 32, 48].

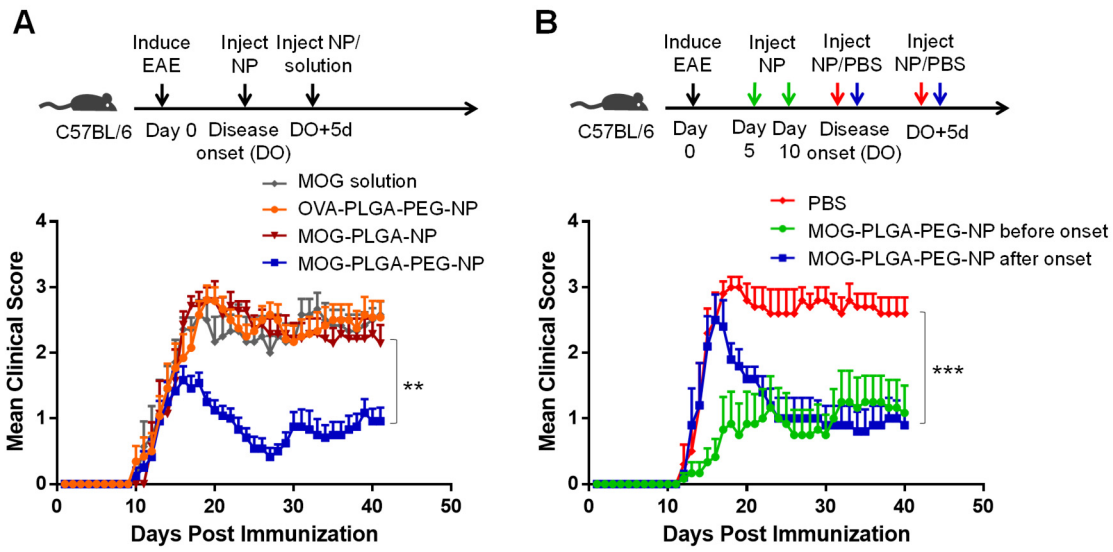

Fig. 3. Induction of antigen-specific tolerance of EAE. (A) Antigen-specific immune tolerance induction via s.c. administration of MOG-PLGA-PEG-NPs. EAE mice were treated at the onset of disease and again 5 days later (MOG_{35-55} solution: n=7; OVA-PLGA-PEG-NPs: n=13; MOG-PLGA-PEG-NPs: n=12; MOG-PLGA-NPs: n=7). (B) Effects of injection timing on NP-induced immune tolerance (n=5~6). Data are represented as mean ± S.E.M. Statistics are shown for the last data point using two-way ANOVA with post-hoc Tukey test. $^{**}p<0.01$; $^{***}p<0.001$.

3.3 PEGylation of NPs reduces stimulatory cellular response in local s.c. tissue

In previous studies of EAE, s.c. injections of autoantigen peptide-containing PLGA-NPs failed to induce tolerance [14, 15, 28]. We performed mechanistic studies to understand the PEGylation-enabled tolerogenic capability of PLGA-NPs. To evaluate subcutaneously administered NPs on cell recruitment and activation, healthy C57BL/6J mice were s.c. injected with 3 mg of DiD-labeled MOG-PLGA-PEG-NPs or MOG-PLGA-NPs. After 48 h, the locally recruited cells around the NP injection site were harvested and stained for CD11c, F4/80, and Ly6G, the classical surface markers of DCs, macrophages, and neutrophils, respectively. Some DCs and macrophages originate from monocytes, expressing both CD11c and F4/80 [49]. Therefore, the $CD11c^{+}F4/80^{-}$ cell population, which is more specific for DCs, was also quantified. The percentages of $CD11c^{+}F4/80^{-}$ cells and $F4/80^{+}$ cells among total recruited cells between mice treated with the two

types of particles were similar (Fig. 4A). Interestingly, a higher percentage of recruited $CD11c^+$ cells in MOG-PLGA-NP-treated mice also expressed F4/80 compared to MOG-PLGA-PEG-NP-treated mice (Fig. S6). It was also found that a significantly higher percentage of neutrophils ($Ly6G^+$) were recruited in mice treated with MOG-PLGA-NPs. The majority of the recruited macrophages internalized NPs (DiD^+) in both treatment conditions, while some $CD11c^+F4/80^-$ cells did not internalize NPs (Fig. S7).

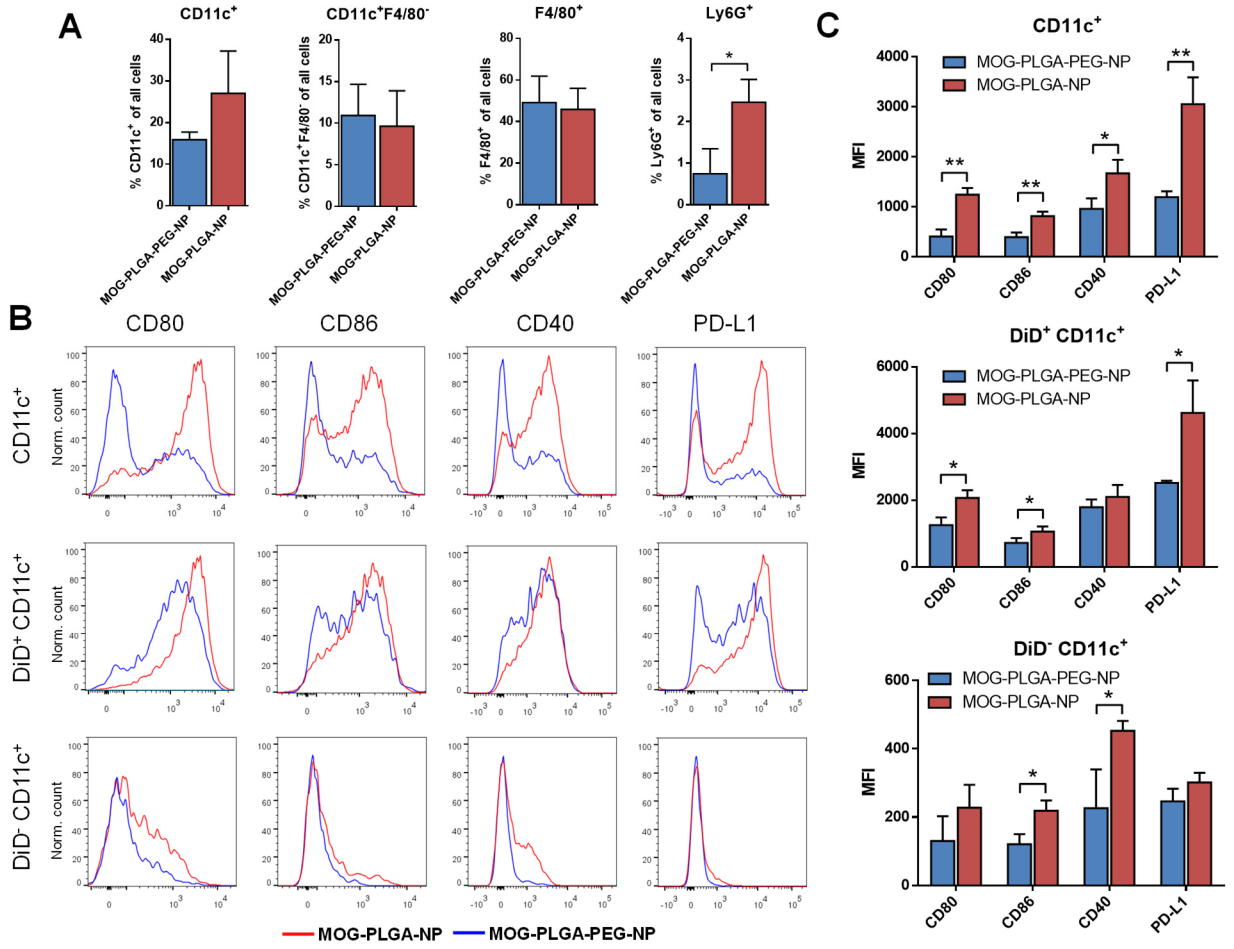

Fig. 4. Local cell recruitment and activation 2 days after s.c. administration of NPs in C57BL/6J mice. (A) Percentage of $CD11c^+$, $CD11c^+$ $F4/80^-$, $F4/80^+$, and $Ly6G^+$ cells surrounding the local NP injection site. (B) Representative flow cytometry histograms of CD80, CD86, CD40, and PD-L1 expression in DCs with and without NP internalization. (C) Mean fluorescence intensity (MFI) of surface markers in each cell population. All data are represented as mean ± S.D. (n=3). *p<0.05; **p<0.01.

Among the $CD11c^+$ cells, we analyzed the expression of CD80, CD86, CD40, and programmed cell death receptor ligand 1 (PD-L1). CD80, CD86, and CD40 are costimulatory signals for T cell activation [4, 50]. PD-L1 is an immunosuppressive regulatory molecule; however, it is often elevated with increased expression of costimulatory molecules in activated APCs [51, 52]. In mice treated with MOG-PLGA-NPs, the level of all four of these markers in $CD11c^+$ cells were significantly higher than those in mice treated with MOG-PLGA-PEG-NPs (Fig. 4B, C). As expected, $CD11c^+$ cells that internalized NPs (DiD^+) had significantly higher CD80, CD86, and PD-L1 in MOG-PLGA-NP-treated mice than in MOG-PLGA-PEG-NP-treated mice. Interestingly, a significantly higher CD86 and CD40 expression was also observed in $CD11c^+$ cells that did not internalize NPs (DiD^-), indicating these cells were affected by their local environment.

3.4 Effects of PEGylation on NP-induced DC and complement activation

To investigate whether PEGylation makes NPs tolerogenic via direct NP-DC interactions, BMDCs were cultured and treated with MOG-PLGA-PEG-NPs and MOG-PLGA-NPs. After 24 h and 48 h, the cells were analyzed for their level of CD80, CD86, and CD40. Interestingly, neither types of NPs activated BMDCs (Fig. 5 and S8). This dissimilarity between *in vitro* and *in vivo* results of DC activation suggests that the response to NPs is more complicated in the *in vivo* environment and may involve factors not present *in vitro*.

Since PEGylation did not have a direct effect on BMDC co-stimulatory marker expression, we hypothesized that other immune components, such as NP-induced complement activation may be involved. Upon contact with the *in vivo* environment, biomolecules including proteins adsorb onto NPs, forming a corona [53]. Complement components can covalently bind to the adsorbed proteins and amplify the complement cascade [54]. The released complement components during activation

recruit and stimulate immune cells, a process generating an inflammatory environment. To gain insight into the complement response to the NPs, MOG-encapsulated NPs were incubated in human serum, which was then analyzed for the presence of complement byproducts C4d and C5a. C4d is correlated with C4 activation found in the classical and lectin pathways. The cleavage of C5 produces C5a, a potent inflammatory chemotactic peptide recruiting immune cells such as neutrophils and monocytes [55]. To ensure uniformity, NPs with a fixed total surface area were mixed with human serum for 1 h, followed by EDTA inactivation and measurement of complement activation by ELISA. IgG and zymosan were used as positive controls. Both C4d and C5a activation was significantly higher in serum containing MOG-PLGA-NPs than that with MOG-PLGA-PEG-NPs (Fig. 6A).

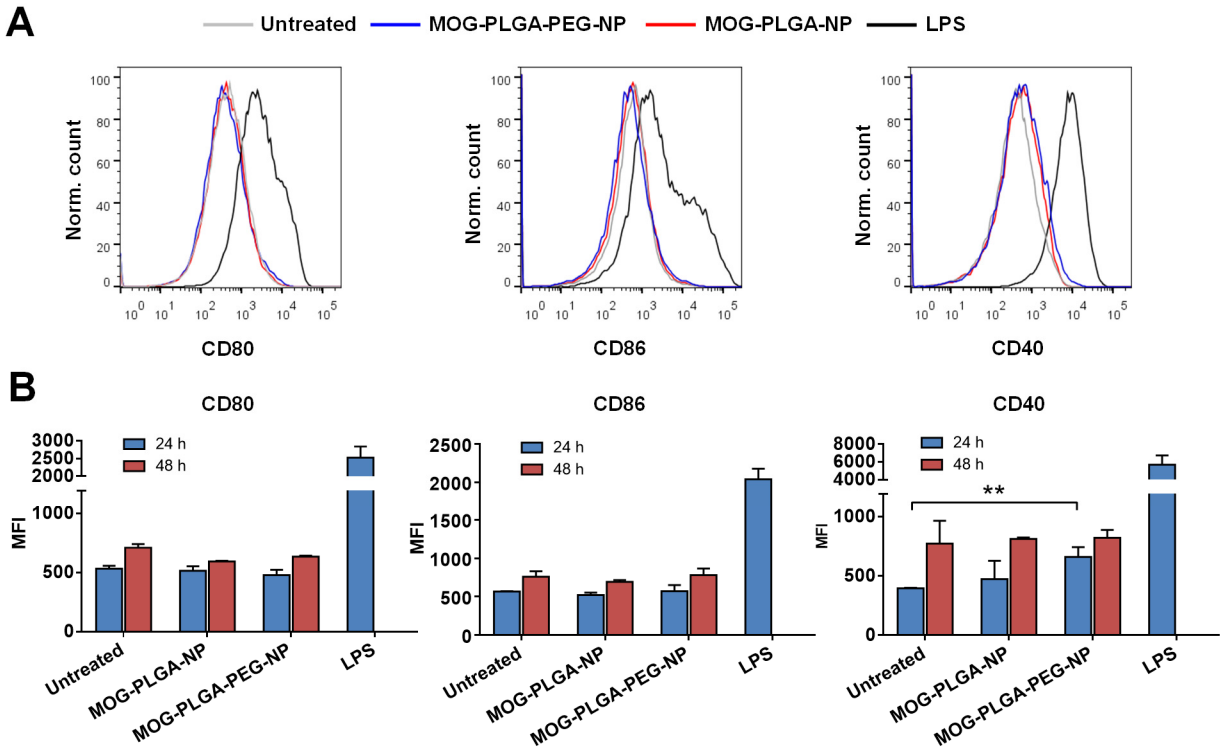

Fig. 5. The effects of PEGylated NPs on dendritic cell activation *in vitro*. (A) Representative flow cytometry histograms of BMDCs (24 h) and (B) marker MFI quantification. BMDCs were cultured and treated on day 6 with 100 μg/mL MOG-PLGA-PEG-NP or MOG-PLGA-NP for 24 h or 48 h before analysis. Data are represented as mean ± S.D. (n=3). *p<0.05; **p<0.01.

To test the *in vivo* complement response to the NP formulations, a healthy mouse was subcutaneously injected with DiD-MOG-PLGA-NPs and DiD-MOG-PLGA-PEG-NPs in different sides of the back. The NPs and NP-infiltrated surrounding tissues were collected 1 h after injection. The amount of complement activation was then characterized via western blot using a monoclonal anti-C3 antibody. The sample containing PLGA-NPs and the surrounding tissue showed a higher intensity of the C3 split product, iC3b compared with that of PLG-PEG-NPs (Fig. 6B). This was determined by the intensity of the α2' chain (40 kDa) (Fig. 6B), which is produced by the splitting of surface-bound C3 by Factor I and reducing agent β-mercaptoethanol. The western blot of skin tissues without any NPs showed α' chain (105kDa) and an unidentified band around 28 kDa. The band representing the α2' chain was unique to the presence of NPs and therefore, was used for the analysis of NP-induced complement activation.

As the first step in immune system activation, the different complement responses likely play a role in downstream immune activation. The decreased complement activation by the PEG layer of NPs together with the reduced neutrophil recruitment and co-stimulatory surface marker expression on DCs, suggest that PEGylation of NPs generated a less inflammatory microenvironment, which is important for inducing tolerogenic responses. Although other factors such as the difference in MOG_{35-55} release rate kinetics from these two NPs (Fig. 2C) may have also contributed to the efficacy difference [56, 57], the difference of release profile is unlikely to dictate the induction of immune tolerance because this and previous studies have shown that free antigen did not ameliorate autoimmunity (Fig. 3A) [17, 58].

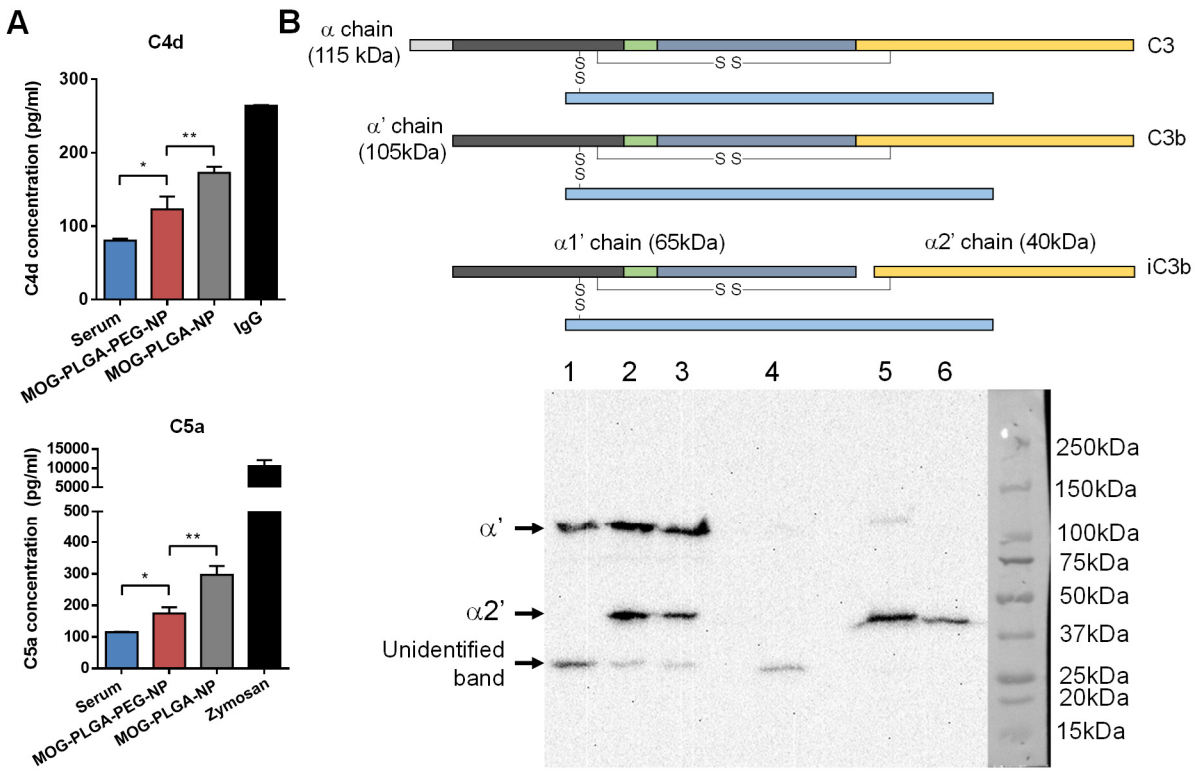

Fig. 6. PEGylation of PLGA-NPs reduces their complement activation *in vitro* and *in vivo*. (A) ELISA measurement of C4d and C5a complement. NPs or heat-aggregated IgG or zymosan (positive controls) were incubated with human serum for 1 h and then inactivated with EDTA. The total NP surface area was 0.05 m^2/mL. Data are represented as mean ± S.D. (n=3~4). *p<0.05; **p<0.01. (B) Representative western blot analysis of NP-induced complement activation *in vivo*. The same amounts of DiD-MOG-PLGA-NPs and DiD-MOG-PLGA-PEG-NPs were s.c. injected into different sides separately on the back of a mouse. After 1 hour, the NPs and NP-infiltrated tissue were collected, analyzed via western blot, and probed with anti-C3 antibody. Amount of C3 activation was determined by the intensity of the band representing the α2' chain. 1. Tissue control supernatant; 2. MOG-PLGA-NP supernatant; 3. MOG-PLGA-PEG-NP supernatant; 4. Tissue control pellet; 5. MOG-PLGA-NP pellet; 6. MOG-PLGA-PEG-NP pellet. This experiment was repeated in 3 separate mice.

3.5 PEGylated NPs have higher localization to APCs in the spleen

We hypothesized that a difference exists in the biodistribution and/or activation of APCs after NP internalization, especially in the APC population in lymphoid organs, in which APCs interact with T cells. To test this, EAE mice were injected s.c. with fluorescent DiD-labeled NPs at the first sign of symptoms (Fig. 7A). To ensure that DiD signal measured was due to NP uptake rather than released DiD, the release rate of DiD from MOG-PLGA and PLGA-PEG NPs in PBS with 10%

FBS was tested at 37 °C. The total amount of DiD signal released in 7 d was less than 5% for both types of particles (Fig. 7B). Six to eight days after s.c. injection of the NPs, cells from the spleen, inguinal and axillary lymph nodes, and central nervous system (CNS) were harvested and analyzed for NP biodistribution and cellular activation markers. This time point was chosen because mice developed EAE between day 10 and day 16 after disease induction and sufficient time was needed for the NPs to be cleared from the injection site and traffic to other organs. Mice were sacrificed either on day 19 or day 21.

Because the NPs are too large to drain to lymph nodes [39], it is likely they were internalized by immune cells and carried to other tissues. Untreated mice were used as a comparison and to gauge autofluorescence signal and noise. Both MOG-PLGA and MOG-PLGA-PEG NPs demonstrated significant localization to the lymph nodes, with 1% of all lymph node cells exhibiting DiD signal (Fig. 7C, S9). The main APC subsets in the lymph nodes were analyzed for DiD signal. DCs ($CD11c^+$) contained the highest percentage of DiD^+ cells, followed closely by macrophages ($F4/80^+$), while only small percentages of neutrophils ($Ly6G^+$) and B cells ($CD19^+$) contained NPs. No differences were detected between the two types of NPs in the percentage of DiD^+ cells of each APC subset.

However, in the spleen, a significantly higher percentage of cells exhibited fluorescence signal of MOG-PLGA-PEG-NPs (Fig. 7D and 7E). Among splenocytes, a higher percentage of macrophages from mice treated with MOG-PLGA-PEG-NPs internalized NPs than those from MOG-PLGA-NP-treated mice. DCs showed the same trend, although there was no statistical significance (p=0.16). Neutrophils and B cells did not exhibit significant differences between the two treatment groups. One possible explanation for the biodistribution result is that MOG-PLGA-NPs were cleared by locally recruited cells, many of which did not traffic to lymphoid organs.

Increased NP presence in splenic cells may be an important attribute of the induced systemic tolerogenic response. In addition, PEGylation of NPs may also affect the spatial distribution of antigen presenting cells within the spleens after their uptake of NPs, a potential mechanism worth further studies in the future.

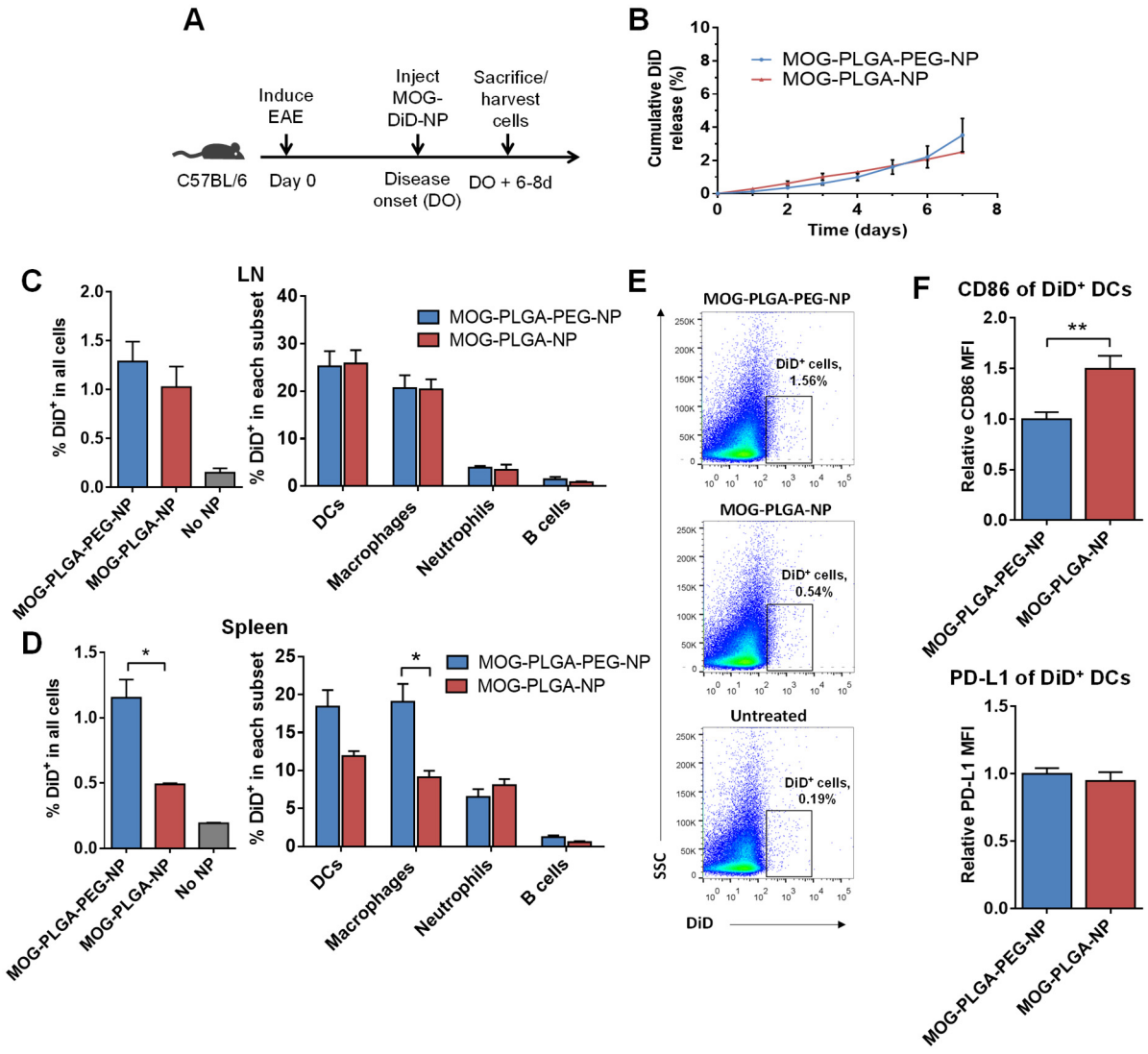

Fig. 7. Biodistribution of NPs in EAE mice. (**A**) Experimental timeline: mice were injected with DiD-labeled NPs at the onset of disease and cells were analyzed 6-8 days later. (**B**) DiD-labeled NPs were tested for DiD release *in vitro*. Data are represented as mean ± S.D. (n=3). (**C**) (**D**) DiD^+ cells in the lymph nodes and spleen. Data are represented as mean ± S.E.M. (MOG-PLGA-PEG-NPs: n=10; MOG-PLGA-NPs: n=3; No NPs: n=3). (**E**) Representative flow cytometry plot of DiD^+ cell gating among all cells in the spleen. (**F**) Splenic DiD^+ DC expression of CD86 and PD-L1. Data are represented as mean ± S.E.M. (n=7). *p<0.05; **p<0.01; ***p<0.001.

The percentage of NP-carrying DCs (DiD^+CD11c^+) was found to be much lower in the CNS than in lymphoid organs for both particles, although more MOG-PLGA-PEG-NP-carrying DCs were observed in the CNS (Fig. S10). The paucity of DCs carrying NPs in the CNS suggests that APCs that internalized NPs exerted their effects in the secondary lymphoid organs away from the primary site of lesions.

The activation status of DCs in the spleen was analyzed by measuring CD86 and PD-L1. DCs containing MOG-PLGA-PEG-NPs exhibited a lower CD86 signal than those containing MOG-PLGA-NPs, although PD-L1 expression was similar between both groups (Fig. 7F). This may be reflective of a more inflammatory response to the MOG-PLGA-NPs in EAE mice. DCs with increased co-stimulatory molecules would have diminished ability to induce tolerogenic T cell responses.

3.6 NP-induced tolerance *in vivo* results in tolerogenic T cell responses

In order to gain insight into the tolerance mechanisms that underlie the amelioration of disease seen with using MOG-PLGA-PEG-NPs, several different measures of T cell responses were studied. To test the antigen-recall ability of NP-treated mice, NPs were s.c. injected into EAE mice at the onset of the disease (Fig. 8A). After 6-8 days, splenocytes were harvested and cultured with MOG_{35-55} peptide for 3 days. Gene transcripts of the splenocytes for the inflammatory cytokines IL-17 and IL-22 were then tested via qRT-PCR. Th17 cells are major contributors of the production of these cytokines and are one of the main pathogenic cell types implicated in EAE and MS [59]. It was found that splenocytes from mice treated with MOG-PLGA-PEG-NPs exhibited a significant reduction in IL-17 and IL-22 transcripts compared to the MOG-PLGA-NP and OVA-

PLGA-PEG-NP-treated groups (Fig. 8B). This indicates that Ag-specific Th17 cells in the spleen of treated mice were either reduced in number or had a suppressed response.

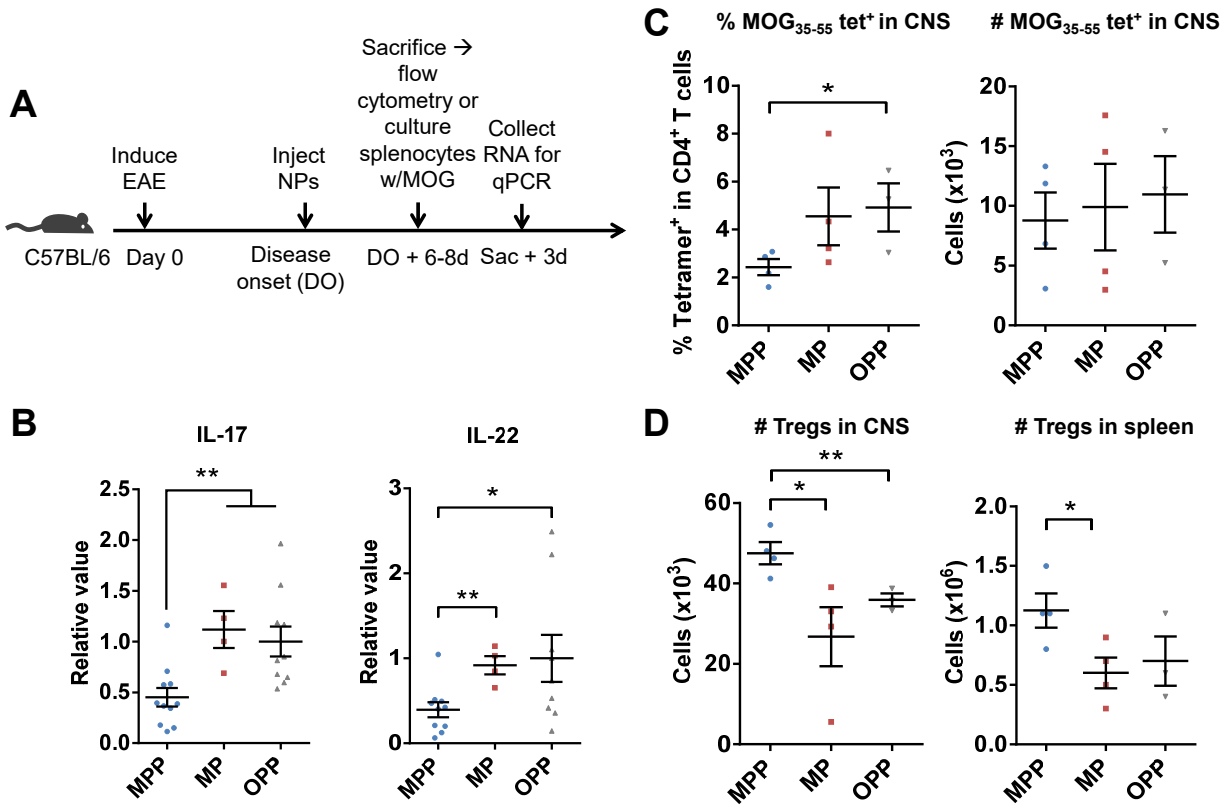

Fig. 8. NP-induced tolerance *in vivo* results in tolerogenic T cell responses. Mice were s.c. injected with MOG-PLGA-PEG-NPs (MPP), MOG-PLGA-NPs (MP), or OVA-PLGA-PEG-NPs (OPP). (A) NPs were injected at the onset of disease. After 6-8 d, CNS and splenocytes were analyzed via flow cytometry or splenocytes were cultured and restimulated with MOG_{35-55} for 3 days. (B) qRT-PCR analysis of splenocyte IL-17 and IL-22 mRNA 3 after restimulation. (C) Percentage and number of MOG_{35-55}-specific CD4 T cells in the CNS. (D) Number of Tregs in the CNS and spleen. Each data point represents one mouse. Data are represented as mean ± S.E.M. *p<0.05; **p<0.01.

Furthermore, to determine whether the reduction in disease score was associated with a decrease in MOG_{35-55}-specific T cells, the T cells from the CNS were harvested 6-8 days after NP injection at the first sign of symptoms. The number of MOG_{35-55}-specific T cells was detected using an I-A(b)MOG_{38-49} tetramer (Fig. S3). MOG-PLGA-PEG-NP-treated mice exhibited a lower overall proportion of MOG_{35-55}-specific T cells among $CD4^+$ T cells than MOG-PLGA-NP and

OVA-PLGA-PEG-NP-treated mice, though statistical significance was only achieved compared to the OVA-PLGA-PEG-NP group (Fig. 8C). However, the absolute number of Ag-specific T cells between the groups exhibited minimal differences. A more pronounced trend was seen in the CNS regulatory T cells (Tregs) ($CD4^+CD25^+FoxP3^+$) population, as MOG-PLGA-PEG-NP-treated mice had significantly higher numbers of Tregs compared to MOG-PLGA-NP and OVA-PLGA-PEG-NP-treated groups (Fig. 8D). In the spleen, a similar trend was observed, though less pronounced (Fig. 8D).

The decrease in number and/or function suppression of Ag-specific Th17 cells in the spleen and increased Tregs in spleen and CNS, and a lower percentage of Ag-specific $CD4^+$ T cells in CNS in MOG-PLGA-PEG-NP-treated mice demonstrate a synergistic response. Taken together, this result suggests that tolerogenic DCs and macrophages that migrate to the spleen from NP injection sites are able to induce Tregs, and the cells migrate to the CNS to exert regulatory effects on Ag-specific pathogenic $CD4^+$ T cells.

4. Conclusion

In summary, we demonstrate that PLGA-PEG-NPs, but not PLGA-NPs with autoantigen peptide alone without tolerogenic drugs can induce antigen-specific immune tolerance after s.c. injection. Important findings associated with the efficacy after NP PEGylation include decreased complement activation and DC co-stimulatory molecule expression *in vivo* and increased NP trafficking to lymph nodes and spleen. Our findings suggest that the DC stimulation *in vivo* by MOG-PLGA-NPs involved factors beyond the direct NP-DC interactions, and the reduction of NP-generated inflammatory microenvironment can be critical for the induction of immune tolerance. The use of NPs for immunomodulation has greatly expanded in recent years. However,

the majority of applications utilize NPs primarily as a delivery vehicle for antigens in combination with tolerogenic or stimulatory molecules, ignoring the intrinsic effect of the particle itself on the immune system. Although studies to reveal the relationship between materials properties and immune responses more specifically are still desired, our study illustrates important factors in nanomaterials design in inducing immune tolerance, particularly via s.c. injection.

Acknowledgements

Research reported in this publication was supported by the National Institute of Allergy and Infectious Diseases of the National Institutes of Health under Award Number R21AI133372, National Science Foundation under Award Numbers 1839505, funding from Pennsylvania Department of Health, CURE grant program, JDRF grant 1-PNF-2018-658-A-N, and a seed funding from the Clinical & Translational Research Institute (CTRI) at Drexel University. The following reagents were obtained through the NIH Tetramer Core Facility: APC-I-A(b) human $CLIP_{87-101}$ tetramer and APC-I-A(b)MOG_{38-49} tetramer.

Declaration of Competing Interest

The authors declare no competing financial interest.

Supplementary data

The Supplementary data is available.

References

[1] A. Davidson, B. Diamond, Advances in immunology - Autoimmune diseases, N. Engl. J. Med., 345 (2001) 340-350.

[2] M.D. Rosenblum, I.K. Gratz, J.S. Paw, A.K. Abbas, Treating Human Autoimmunity: Current Practice and Future Prospects, Sci. Transl. Med., 4 (2012) 10.

[3] E. Montes-Cobos, S. Ring, H.J. Fischer, J. Heck, J. Strauss, M. Schwaninger, S.D. Reichardt, C. Feldmann, F. Luhder, H.M. Reichardt, Targeted delivery of glucocorticoids to macrophages in a mouse model of multiple sclerosis using inorganic-organic hybrid nanoparticles, J. Control. Release, 245 (2017) 157-169.

[4] S.D. Miller, D.M. Turley, J.R. Podojil, Antigen-specific tolerance strategies for the prevention and treatment of autoimmune disease, Nat. Rev. Immunol., 7 (2007) 665-677.

[5] M.P. Domogalla, P.V. Rostan, V.K. Raker, K. Steinbrink, Tolerance through education: How Tolerogenic Dendritic Cells Shape immunity, Front. Immunol., 8 (2017) 14.

[6] H. Hasegawa, T. Matsumoto, Mechanisms of Tolerance induction by Dendritic Cells In Vivo, Front. Immunol., 9 (2018) 14.

[7] D.S. Wilson, M. Damo, S. Hirosue, M.M. Raczy, K. Brunggel, G. Diaceri, X. Quaglia-Thermes, J.A. Hubbell, Synthetically glycosylated antigens induce antigen-specific tolerance and prevent the onset of diabetes, Nat. Biomed. Eng., 3 (2019) 817-829.

[8] J.M. Gammon, C.M. Jewell, Engineering Immune Tolerance with Biomaterials, Adv. Healthc. Mater., 8 (2019) 19.

[9] L.H. Tostanoski, Y.C. Chiu, J.M. Gammon, T. Simon, J.I. Andorko, J.S. Bromberg, C.M. Jewell, Reprogramming the Local Lymph Node Microenvironment Promotes Tolerance that Is Systemic and Antigen Specific, Cell Rep., 16 (2016) 2940-2952.

[10] A. Yeste, M. Nadeau, E.J. Burns, H.L. Weiner, F.J. Quintana, Nanoparticle-mediated codelivery of myelin antigen and a tolerogenic small molecule suppresses experimental autoimmune encephalomyelitis, Proc. Natl. Acad. Sci. U. S. A., 109 (2012) 11270-11275.

[11] C. Capini, M. Jaturanpinyo, H.I. Chang, S. Mutalik, A. McNally, S. Street, R. Steptoe, B. O'Sullivan, N. Davies, R. Thomas, Antigen-Specific Suppression of Inflammatory Arthritis Using Liposomes, J. Immunol., 182 (2009) 3556-3565.

[12] A.S. Bergot, I. Buckle, S. Cikaluru, J.L. Naranjo, C.M. Wright, G.L. Zheng, M. Talekar, E.E. Hamilton-Williams, R. Thomas, Regulatory T Cells Induced by Single-Peptide Liposome Immunotherapy Suppress Islet-Specific T Cell Responses to Multiple Antigens and Protect from Autoimmune Diabetes, J. Immunol., 204 (2020) 1787-1797.

[13] X. Clemente-Casares, J. Blanco, P. Ambalavanan, J. Yamanouchi, S. Singha, C. Fandos, S. Tsai, J.G. Wang, N. Garabatos, C. Izquierdo, S. Agrawal, M.B. Keough, V.W. Yong, E. James, A. Moore, Y. Yang, T. Stratmann, P. Serra, P. Santamaria, Expanding antigen-specific regulatory networks to treat autoimmunity, Nature, 530 (2016) 434-440.

[14] D.R. Getts, A.J. Martin, D.P. McCarthy, R.L. Terry, Z.N. Hunter, W.T. Yap, M.T. Getts, M. Pleiss, X.R. Luo, N.J.C. King, L.D. Shea, S.D. Miller, Microparticles bearing encephalitogenic peptides induce T-cell tolerance and ameliorate experimental autoimmune encephalomyelitis, Nat. Biotechnol., 30 (2012) 1217-1224.

[15] Z. Hunter, D.P. McCarthy, W.T. Yap, C.T. Harp, D.R. Getts, L.D. Shea, S.D. Miller, A Biodegradable Nanoparticle Platform for the Induction of Antigen-Specific Immune Tolerance for Treatment of Autoimmune Disease, ACS Nano, 8 (2014) 2148-2160.

[16] R.A. Maldonado, R.A. LaMothe, J.D. Ferrari, A.H. Zhang, R.J. Rossi, P.N. Kolte, A.P. Griset, C. O'Neil, D.H. Altreuter, E. Browning, L. Johnston, O.C. Farokhzad, R. Langer, D.W. Scott, U.H. von Andrian, T.K. Kishimoto, Polymeric synthetic nanoparticles for the induction of antigen-specific immunological tolerance, Proc. Natl. Acad. Sci. U. S. A., 112 (2015) E156-E165.
[17] N. Pishesha, A.M. Bilate, M.C. Wibowo, N.J. Huang, Z.Y. Li, R. Dhesycka, D. Bousbaine, H.J. Li, H.C. Patterson, S.K. Dougan, T. Maruyama, H.F. Lodish, H.L. Ploegh, Engineered erythrocytes covalently linked to antigenic peptides can protect against autoimmune disease, Proc. Natl. Acad. Sci. U. S. A., 114 (2017) 3157-3162.
[18] S. Kontos, I.C. Kourtis, K.Y. Dane, J.A. Hubbell, Engineering antigens for in situ erythrocyte binding induces T-cell deletion, Proc. Natl. Acad. Sci. U. S. A., 110 (2013) E60-E68.
[19] E. Saito, R. Kuo, K.R. Kramer, N. Gohel, D.A. Giles, B.B. Moore, S.D. Miller, L.D. Shea, Design of biodegradable nanoparticles to modulate phenotypes of antigen-presenting cells for antigen-specific treatment of autoimmune disease, Biomaterials, 222 (2019) 119432.
[20] Q. Liu, X. Wang, X.S. Liu, S. Kumar, G. Gochman, Y. Ji, Y.P. Liao, C.H. Chang, W. Situ, J.Q. Lu, J.H. Jiang, K.C. Mei, H. Meng, T. Xia, A.E. Nel, Use of Polymeric Nanoparticle Platform Targeting the Liver To Induce Treg-Mediated Antigen-Specific Immune Tolerance in a Pulmonary Allergen Sensitization Model, ACS Nano, 13 (2019) 4778-4794.
[21] G. Casella, J. Rasouli, A. Boehm, W.F. Zhang, D. Xiao, L.L.W. Ishikawa, R. Thome, X. Li, D. Hwang, P. Porazzi, S. Molugu, H.Y. Tang, G.X. Zhang, B. Ciric, A. Rostami, Oligodendrocyte-derived extracellular vesicles as antigen-specific therapy for autoimmune neuroinflammation in mice, Sci. Transl. Med., 12 (2020) 13.
[22] N.J. Shah, A.S. Mao, T.Y. Shih, M.D. Kerr, A. Sharda, T.M. Raimondo, J.C. Weaver, V.D. Vrbanac, M. Deruaz, A.M. Tager, D.J. Mooney, D.T. Scadden, An injectable bone marrow-like scaffold enhances T cell immunity after hematopoietic stem cell transplantation, Nat. Biotechnol., 37 (2019) 293-302.
[23] M.O. Dellacherie, B.R. Seo, D.J. Mooney, Macroscale biomaterials strategies for local immunomodulation, Nat. Rev. Mater., 4 (2019) 379-397.
[24] J.S. Lewis, J.M. Stewart, G.P. Marsha, M.R. Carstens, Y. Zhang, N.V. Dolgoya, C.Q. Xia, T.M. Brusko, C.H. Wasserfall, M.J. Clare-Salzler, M.A. Atkinson, B.G. Keselowsky, Dual-Sized Microparticle System for Generating Suppressive Dendritic Cells Prevents and Reverses Type 1 Diabetes in the Nonobese Diabetic Mouse Model, ACS Biomater. Sci. Eng., 5 (2019) 2631-2646.
[25] S.C. Balmert, C. Donahue, J.R. Vu, G. Erdos, L.D. Falo, S.R. Little, In vivo induction of regulatory T cells promotes allergen tolerance and suppresses allergic contact dermatitis, J. Control. Release, 261 (2017) 223-233.
[26] R. Aharoni, A. Herschkovitz, R. Eilam, M. Blumberg-Hazan, M. Sela, W. Bruck, R. Arnon, Demyelination arrest and remyelination induced by glatiramer acetate treatment of experimental autoimmune encephalomyelitis, Proc. Natl. Acad. Sci. U. S. A., 105 (2008) 11358-11363.
[27] T. Prod'homme, S.S. Zamvil, The Evolving Mechanisms of Action of Glatiramer Acetate, Cold Spring Harbor Perspectives in Medicine, 9 (2019) 15.
[28] G. Cappellano, A.D. Woldetsadik, E. Orilieri, Y. Shivakumar, M. Rizzi, F. Carniato, C.L. Gigliotti, E. Boggio, N. Clemente, C. Comi, C. Dianzani, R. Boldorini, A. Chiocchetti, F. Reno, U. Dianzani, Subcutaneous inverse vaccination with PLGA particles loaded with a MOG

peptide and IL-10 decreases the severity of experimental autoimmune encephalomyelitis, Vaccine, 32 (2014) 5681-5689.
[29] J.J. Cho, J.M. Stewart, T.T. Drashansky, M.A. Brusko, A.N. Zuniga, K.J. Lorentsen, B.G. Keselowsky, D. Avram, An antigen-specific semi-therapeutic treatment with local delivery of tolerogenic factors through a dual-sized microparticle system blocks experimental autoimmune encephalomyelitis, Biomaterials, 143 (2017) 79-92.
[30] K.J. Peine, M. Guerau-de-Arellano, P. Lee, N. Kanthamneni, M. Severin, G.D. Probst, H.Y. Peng, Y.H. Yang, Z. Vangundy, T.L. Papenfuss, A.E. Lovett-Racke, E.M. Bachelder, K.M. Ainslie, Treatment of Experimental Autoimmune Encephalomyelitis by Codelivery of Disease Associated Peptide and Dexamethasone in Acetalated Dextran Microparticles, Mol. Pharm., 11 (2014) 828-835.
[31] L.H. Tostanoski, Y.C. Chiu, J.I. Andorko, M. Guo, X.B. Zeng, P.P. Zhang, W. Royal, C.M. Jewell, Design of Polyelectrolyte Multilayers to Promote Immunological Tolerance, ACS Nano, 10 (2016) 9334-9345.
[32] L.M. Casey, R.M. Pearson, K.R. Hughes, J.M.H. Liu, J.A. Rose, M.G. North, L.Z. Wang, M. Lei, S.D. Miller, L.D. Shea, Conjugation of Transforming Growth Factor Beta to Antigen-Loaded Poly(lactide-co-glycolide) Nanoparticles Enhances Efficiency of Antigen-Specific Tolerance, Bioconjugate Chem., 29 (2018) 813-823.
[33] J.M. Gammon, L.H. Tostanoski, A.R. Adapa, Y.C. Chiu, C.M. Jewell, Controlled delivery of a metabolic modulator promotes regulatory T cells and restrains autoimmunity, J. Control. Release, 210 (2015) 169-178.
[34] L. Northrup, J.D. Griffin, M.A. Christopher, L.R. Antunez, B.L. Hartwell, C.J. Pickens, C. Berkland, Co-delivery of autoantigen and dexamethasone in incomplete Freund's adjuvant ameliorates experimental autoimmune encephalomyelitis, J. Control. Release, 266 (2017) 156-165.
[35] N. Benne, R.J.T. Leboux, M. Glandrup, J. van Duijn, F.L. Vigario, M.A. Neustrup, S. Romeijn, F. Galli, J. Kuiper, W. Jiskoot, B. Slutter, Atomic force microscopy measurements of anionic liposomes reveal the effect of liposomal rigidity on antigen-specific regulatory T cell responses, J. Control. Release, 318 (2020) 246-255.
[36] Y.Z. Min, K.C. Roche, S.M. Tian, M.J. Eblan, K.P. McKinnon, J.M. Caster, S.J. Chai, L.E. Herring, L.Z. Zhang, T. Zhang, J.M. DeSimone, J.E. Tepper, B.G. Vincent, J.S. Serody, A.Z. Wang, Antigen-capturing nanoparticles improve the abscopal effect and cancer immunotherapy, Nat. Nanotechnol., 12 (2017) 877-882.
[37] Z.Y. Fan, P.Y. Li, J.J. Deng, S.C. Bady, H. Cheng, Cell membrane coating for reducing nanoparticle-induced inflammatory responses to scaffold constructs, Nano Res., 11 (2018) 5573-5583.
[38] B. Nilsson, K.N. Ekdahl, T.E. Mollnes, J.D. Lambris, The role of complement in biomaterial-induced inflammation, Mol. Immunol., 44 (2007) 82-94.
[39] S.T. Reddy, A.J. van der Vlies, E. Simeoni, V. Angeli, G.J. Randolph, C.P. O'Neill, L.K. Lee, M.A. Swartz, J.A. Hubbell, Exploiting lymphatic transport and complement activation in nanoparticle vaccines, Nat. Biotechnol., 25 (2007) 1159-1164.
[40] T.H. Ding, J. Guan, M.K. Wang, Q.Q. Long, X. Liu, J. Qian, X.L. Wei, W.Y. Lu, C.Y. Zhan, Natural IgM dominates in vivo performance of liposomes, J. Control. Release, 319 (2020) 371-381.
[41] G. Gifford, V.P. Vu, N.K. Banda, V.M. Holers, G.K. Wang, E.V. Groman, D. Backos, R. Scheinman, S.M. Moghimi, D. Simberg, Complement therapeutics meets nanomedicine:

overcoming human complement activation and leukocyte uptake of nanomedicines with soluble domains of CD55, J. Control. Release, 302 (2019) 181-189.
[42] J.S. Suk, Q.G. Xu, N. Kim, J. Hanes, L.M. Ensign, PEGylation as a strategy for improving nanoparticle-based drug and gene delivery, Adv. Drug Deliv. Rev., 99 (2016) 28-51.
[43] H. Zhou, Z.Y. Fan, P.Y. Li, J.J. Deng, D.C. Arhontoulis, C.Y. Li, W.B. Bowne, H. Cheng, Dense and Dynamic Polyethylene Glycol Shells Cloak Nanoparticles from Uptake by Liver Endothelial Cells for Long Blood Circulation, ACS Nano, 12 (2018) 10130-10141.
[44] Z. Fan, P. Zhu, Y. Zhu, K. Wu, C.Y. Li, H. Cheng, Engineering long-circulating nanomaterial delivery systems, Curr. Opin. Biotechnol., 66 (2020) 131-139.
[45] G. Cappellano, C. Comi, A. Chiocchetti, U. Dianzani, Exploiting PLGA-Based Biocompatible Nanoparticles for Next-Generation Tolerogenic Vaccines against Autoimmune Disease, International Journal of Molecular Sciences, 20 (2019) 204.
[46] R. Rietscher, J.A. Czaplewska, T.C. Majdanski, M. Gottschaldt, U.S. Schubert, M. Schneider, C.M. Lehr, Impact of PEG and PEG-b-PAGE modified PLGA on nanoparticle formation, protein loading and release, Int. J. Pharm., 500 (2016) 187-195.
[47] M.B. Lutz, N. Kukutsch, A.L.J. Ogilvie, S. Rossner, F. Koch, N. Romani, G. Schuler, An advanced culture method for generating large quantities of highly pure dendritic cells from mouse bone marrow, J. Immunol. Methods, 223 (1999) 77-92.
[48] T.K. Kishimoto, J.D. Ferrari, R.A. LaMothe, P.N. Kolte, A.P. Griset, C. O'Neil, V. Chan, E. Browning, A. Chalishazar, W. Kuhlman, F.N. Fu, N. Viseux, D.H. Altreuter, L. Johnston, R.A. Maldonado, Improving the efficacy and safety of biologic drugs with tolerogenic nanoparticles, Nat. Nanotechnol., 11 (2016) 890-899.
[49] E.L. Gautier, T. Shay, J. Miller, M. Greter, C. Jakubzick, S. Ivanov, J. Helft, A. Chow, K.G. Elpek, S. Gordonov, A.R. Mazloom, A. Ma'ayan, W.J. Chua, T.H. Hansen, S.J. Turley, M. Merad, G.J. Randolph, C. Immunological Genome, Gene-expression profiles and transcriptional regulatory pathways that underlie the identity and diversity of mouse tissue macrophages, Nature Immunology, 13 (2012) 1118-1128.
[50] D.Y. Ma, E.A. Clark, The role of CD40 and CD154/CD40L in dendritic cells, Seminars in Immunology, 21 (2009) 265-272.
[51] A.V. Bazhin, K. von Ahn, J. Fritz, J. Werner, S. Karakhanova, Interferon-alpha Up-Regulates the Expression of PD-L1 Molecules on Immune Cells Through STAT3 and p38 Signaling, Front. Immunol., 9 (2018) 2129.
[52] V. Pulko, X. Liu, C.J. Krco, K.J. Harris, X. Frigola, E.D. Kwon, H.D. Dong, TLR3-Stimulated Dendritic Cells Up-regulate B7-H1 Expression and Influence the Magnitude of CD8 T Cell Responses to Tumor Vaccination, J. Immunol., 183 (2009) 3634-3641.
[53] M.P. Monopoli, C. Aberg, A. Salvati, K.A. Dawson, Biomolecular coronas provide the biological identity of nanosized materials, Nat. Nanotechnol., 7 (2012) 779-786.
[54] F.F. Chen, G.K. Wang, J.I. Griffin, B. Brenneman, N.K. Banda, V.M. Holers, D.S. Backos, L.P. Wu, S.M. Moghimi, D. Simberg, Complement proteins bind to nanoparticle protein corona and undergo dynamic exchange in vivo, Nat. Nanotechnol., 12 (2017) 387-393.
[55] P.F. Zipfel, C. Skerka, Complement regulators and inhibitory proteins, Nat. Rev. Immunol., 9 (2009) 729-740.
[56] P. Johansen, T. Storni, L. Rettig, Z.Y. Qiu, A. Der-Sarkissian, K.A. Smith, V. Manolova, K.S. Lang, G. Senti, B. Mullhaupt, T. Gerlach, R.F. Speck, A. Bot, T.M. Kundig, Antigen kinetics determines immune reactivity, Proc. Natl. Acad. Sci. U. S. A., 105 (2008) 5189-5194.

[57] A. Mayer, Y.J. Zhang, A.S. Perelson, N.S. Wingreen, Regulation of T cell expansion by antigen presentation dynamics, Proc. Natl. Acad. Sci. U. S. A., 116 (2019) 5914-5919.
[58] A. Carambia, B. Freund, D. Schwinge, O.T. Bruns, S.C. Salmen, H. Ittrich, R. Reimer, M. Heine, S. Huber, C. Waurisch, A. Eychmuller, D.C. Wraith, T. Korn, P. Nielsen, H. Weller, C. Schramm, S. Luth, A.W. Lohse, J. Heeren, J. Herkel, Nanoparticle-based autoantigen delivery to Treg-inducing liver sinusoidal endothelial cells enables control of autoimmunity in mice, J. Hepatol., 62 (2015) 1349-1356.
[59] E. Bettelli, T. Korn, M. Oukka, V.K. Kuchroo, Induction and effector functions of T(H)17 cells, Nature, 453 (2008) 1051-1057.